

# Effect of Second Phase on the Deformation and Fracture Behavior of Multiphase Low-Density Steels

SEONG-JUN PARK,<sup>1</sup> YOON-UK HEO,<sup>2</sup> YONG HOON CHOI,<sup>2</sup>  
KEUNHO LEE,<sup>3</sup> HEUNG NAM HAN,<sup>3</sup> and DONG-WOO SUH<sup>2,4</sup>

1.—Ferrous Alloy Department, Korea Institute of Materials Science, Changwon, Korea. 2.—Graduate Institute of Ferrous Technology, Pohang University of Science and Technology, Pohang, Korea. 3.—Department of Materials Science and Engineering, Seoul National University, Seoul, Korea. 4.—e-mail: dongwoo1@postech.ac.kr

The effects of the second-phase characteristics on the deformation and fracture behavior in low-density steel are investigated in Fe-0.2C-(4, 8)Mn-5Al-1Si alloys, where the second phase can be retained austenite or a mixture of  $\kappa$ -carbide and ferrite depending on the processing condition. With austenite as second phase, the mechanical stability of the austenite is critical regarding ductility because the fracture is likely to occur before the onset of necking when the austenite transforms into martensite in the early stage of deformation. In the case of the mixture of ferrite and  $\kappa$ -carbide, the round shape of  $\kappa$ -carbide is more favorable than the dense lamellar structure. The prominent influence of the second phase on the deformation and fracture behavior is attributable to the propensity of matrix ferrite for cleavage fracture due to its large aluminum concentration.

## INTRODUCTION

Increasing strength without compromising ductility has been a successful strategy in the development of automobile materials, hence, the huge activity in the development of the so-called advanced high-strength steels.<sup>1–3</sup> However, high strength can only be exploited in the context of light-weighting if the structural stiffness of the thinner sections used is not unacceptable. Stiffness determines vibration modes and crash performance of the automobile.

A way of ameliorating these problems is to reduce the density of steel by alloying with light elements such as aluminum while maintaining their strength.<sup>4–6</sup> The aluminum-added low-density steels can be categorized into ferritic, austenitic, and multiphase steels with respect to the constituent phases.<sup>7–10</sup> The multiphase variety can contain retained austenite,  $\kappa$ -carbide, martensite, or mixtures of these phases.<sup>11–13</sup> It is useful therefore to conduct a systematic study on the role of the second phase; in the present work, the consequences on mechanical performance are studied using Fe-0.2C-(4, 8) Mn-5Al-1Si alloys, in which an approximately 6% of density reduction is expected.<sup>14</sup> The overall

microstructure can be manipulated by changing the isothermal heat treatment time because the retained austenite can be induced to gradually decompose into ferrite and  $\kappa$ -carbide. The mechanical stability of austenite and the distribution and morphology of  $\kappa$ -carbide on the deformation and fracture behavior of the alloys are examined.

## EXPERIMENTAL METHODS

Table I shows the chemical composition of investigated alloys. Alloys A and B are almost the same except the difference in manganese content of 4 wt.% and 8 wt.%, respectively.

After vacuum melting of 25-kg ingots, they were heated to 1200°C for 1 h and hot-rolled to a 3.2-mm-thick sheet with a final rolling temperature above 870°C. After hot rolling, the sheets were held at 650°C for 1 h to simulate the coiling process followed by furnace cooling to room temperature. The sheets were heat treated using an infrared heating furnace as shown in Fig. 1, where the holding time at 600°C was varied to control the second phase. The microstructure was examined on the plane containing rolling and normal directions using scanning electron microscopy (SEM) with electron

back-scatter diffraction (EBSD). A standard method consisting of mechanical polishing and etching with 2% nital solution was used for metallographic analysis. For the EBSD measurement, the specimens were finally polished with colloidal silica and a step size of 0.1  $\mu\text{m}$  or 0.15  $\mu\text{m}$  was used for phase mapping. Transmission electron microscopy (TEM) specimens were prepared by electro-chemical polishing in a 10% perchloric acid +90% acetic acid solution maintained at room temperature and a constant voltage of 50 V. The austenite fraction was measured with x-ray diffraction using Cu-K $\alpha$  radiation with graphite monochromator. The specimens were prepared by mechanical grinding followed by chemical polishing in 4% HF + H $_2$ O $_2$  solution to remove the deformed layer. The austenite fraction was calculated with integrated intensity of (200) $_{\alpha}$ , (211) $_{\alpha}$  and (220) $_{\gamma}$  and (311) $_{\gamma}$  using a direct comparison method.<sup>15</sup> Tensile tests were conducted using sub-sized specimens according to ASTM E8M

**Table I. Chemical composition of investigated alloys (wt.%)**

Alloy	C	Mn	Al	Si	Fe
A	0.21	4.1	5.0	1.0	Bal.
B	0.21	8.1	5.0	1.0	Bal.

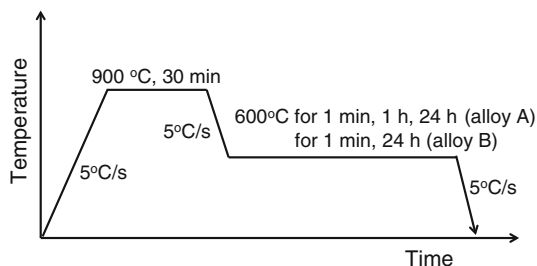


Fig. 1. Heat treatment conditions.

specification at a crosshead speed of 2 mm/min. The fractured surface and the microstructure of adjacent fractured region after tensile test were observed using SEM to investigate the occurrence of crack and propagation.

## RESULTS AND DISCUSSION

### Microstructure and Tensile Properties

Figure 2 shows the equilibrium phase fractions as a function of temperature, estimated using calculation of phase diagram (CALPHAD) method.<sup>16</sup> The alloys investigated are in two-phase region consisting of ferrite and austenite at 900°C. The fraction of austenite gradually decreases with temperature, as it decomposes into a mixture of ferrite and  $\kappa$ -carbide during isothermal heat-treatment at 600°C. In alloy B, which contains a greater manganese concentration, the austenite remains stable at 600°C.<sup>17</sup> The microstructural evolution in alloy A, observed using scanning electron microscopy, is shown in Fig. 3a, b and c. As the isothermal time elapses, the initial austenite is converted gradually into a lamellar structure. Judging from the thermodynamic calculation in Fig. 2, the austenite will decompose into ferrite and  $\kappa$ -carbide on holding at the temperature for a long enough time. Following the decomposition of austenite, the  $\kappa$ -carbide lamellae are observed at 24 h to spheroidize. A similar trend is found for alloy B in Fig. 3d and e. It is noted that the austenite fraction in alloy B at the earlier stage of isothermal treatment is larger compared with the alloy A and a considerable amount of austenite is likely to remain even after isothermal treatment of 24 h, which is consistent with the thermodynamic calculation in Fig. 2. Table II summarizes the austenite fraction evaluated using x-ray diffraction.

Figure 4 presents the EBSD phase map overlaid with image quality data, taking only account of face-centered cubic (FCC) and body-centered cubic (BCC) structures. The phase map confirms the presence of austenite at 1 min of isothermal heat-treatment in both alloys and the retention of austenite after

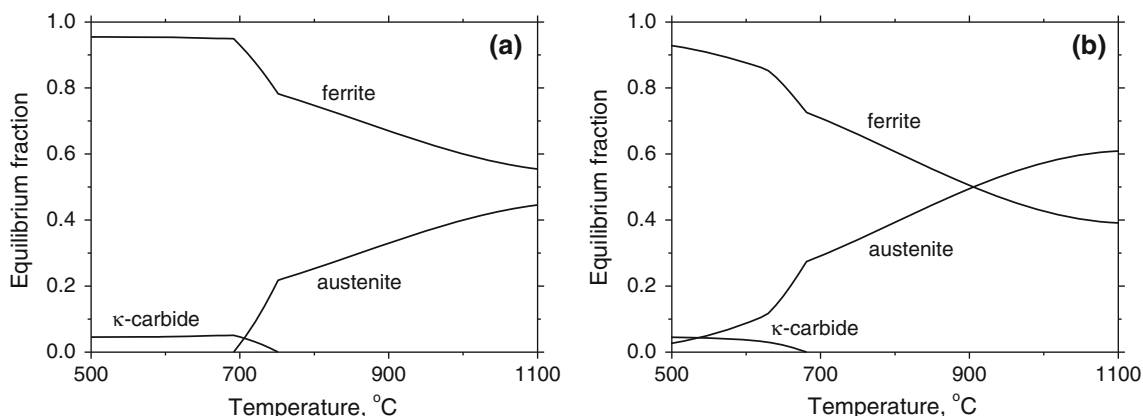


Fig. 2. Equilibrium fraction calculated with CALPHAD method.

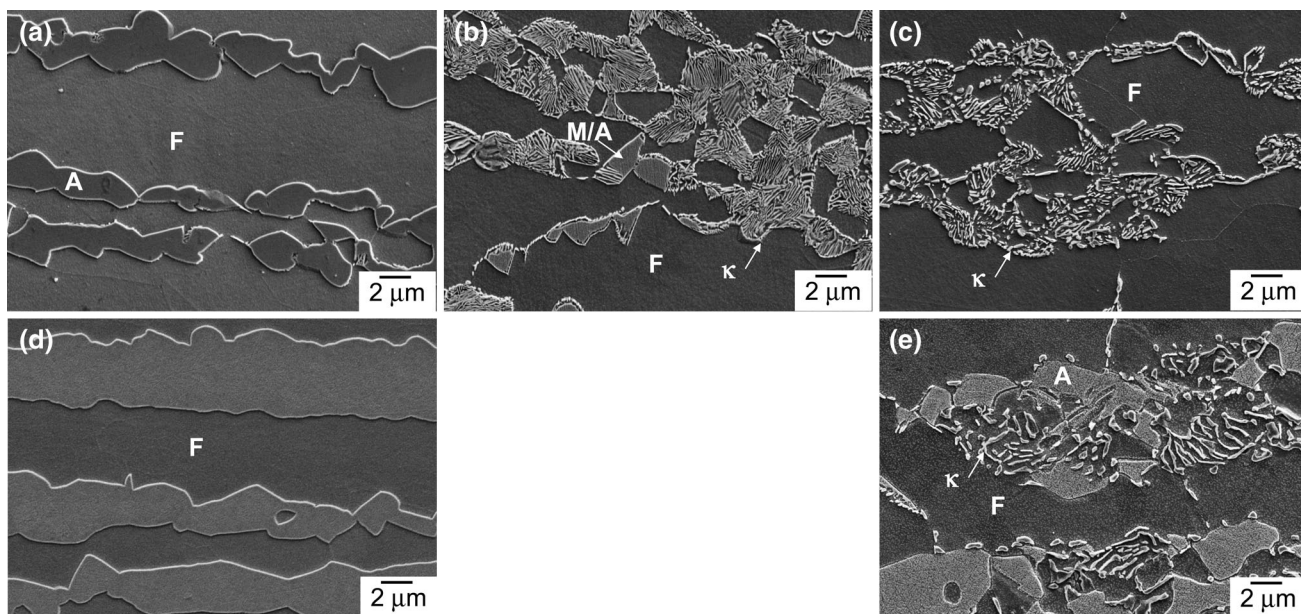


Fig. 3. SEM micrographs of alloy A isothermally heat treated for (a) 1 min, (b) 1 h, and (c) 24 h and alloy B for (d) 1 min and (e) 24 h. (F, A, M, and  $\kappa$  represent ferrite, austenite, martensite, and  $\kappa$ -carbide, respectively).

**Table II. Austenite fraction and mechanical properties after isothermal heat treatment**

Alloy	Isothermal heat treatment time	Austenite fraction (%)	Yield strength (MPa)	Tensile strength (MPa)	Total elongation (%)
A	1 min	9.1	551	693	13.9
A	1 h	3.0	571	782	10.9
A	24 h	—	537	816	30.3
B	1 min	19.3	532	710	37.4
B	24 h	10.5	559	803	31.9

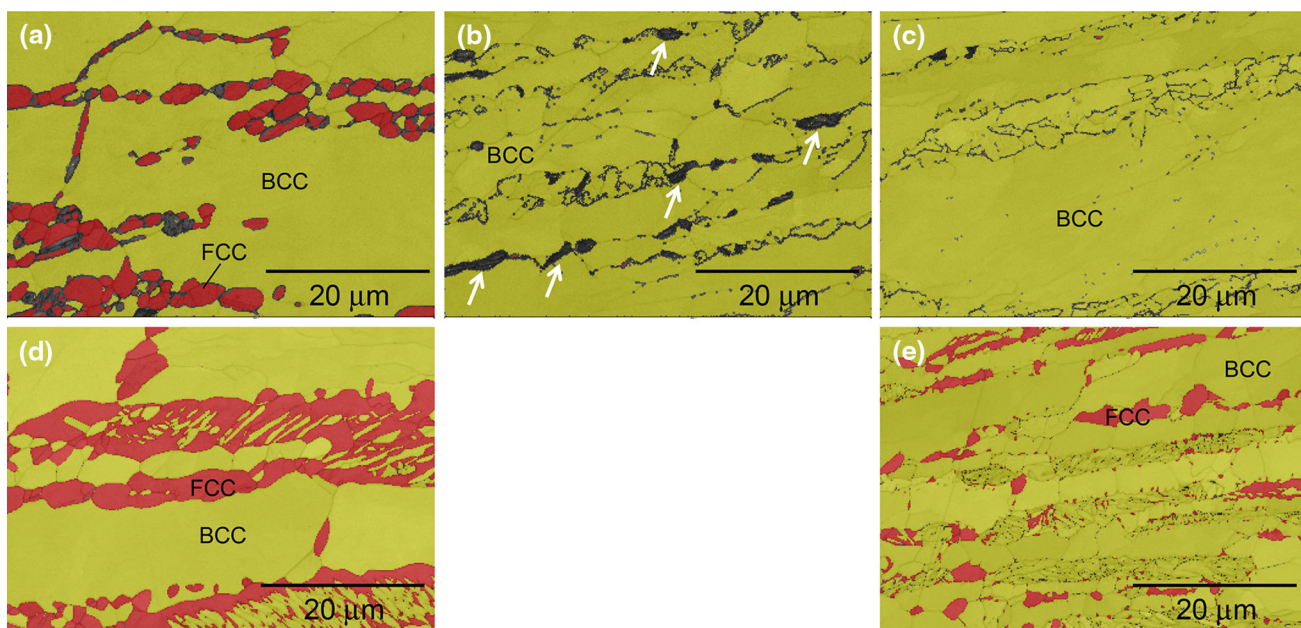


Fig. 4. EBSD phase map of alloy A isothermally heat treated for (a) 1 min, (b) 1 h, and (c) 24 h and alloy B for (d) 1 min and (e) 24 h.



isothermal treatment of 24 h in alloy B. Meanwhile, it is noteworthy that microstructural features that have quite low image quality are observed in alloy A after isothermal treatment of 1 h (indicated with arrows in Fig. 4b). Given that it is recognized as a BCC structure but has lower image quality, it is thought to be martensite, which should have poor image quality because of high dislocation density.<sup>18</sup> The formation of martensite is possibly because of the change of carbon concentration in austenite as  $\kappa$ -carbide absorbs carbon. In alloy B, a microstructure constituent regarded as martensite is not observed after isothermal treatment of 24 h where austenite coexists with  $\kappa$ -carbide. It is attributed to the better stability of austenite originating from higher manganese content.

Figure 5 compares the stress–strain curves of investigated alloys, and the result is summarized in Table II. In alloy A subjected to isothermal treatment of 1 min and 1 h, the fracture happens before the occurrence of necking, so overall elongation is less than 15%. Considerable uniform deformation is observed in alloy A after isothermal treatment of 24 h. Fracture before necking does not occur and total elongation over 30% is obtained in alloy B subjected to the isothermal treatment of 1 min and 24 h. The corresponding fracture surface is shown in Fig. 6. Severe cleavage facets are observed in alloy A isothermally treated for 1 min and 1 h in Fig. 6a and b, indicating lack of ability to accommodate the deformation in both matrix and second phases. On the other hand, in cases where the

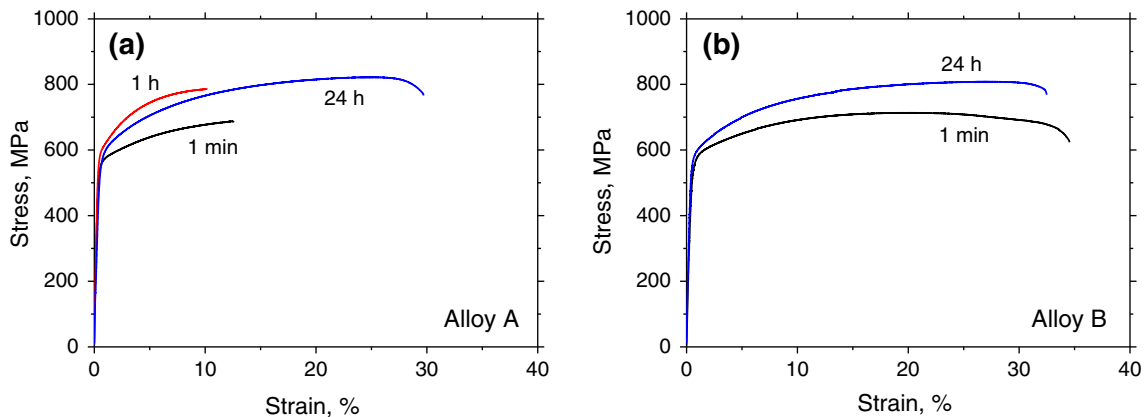


Fig. 5. Stress–strain curves of (a) alloy A and (b) alloy B.

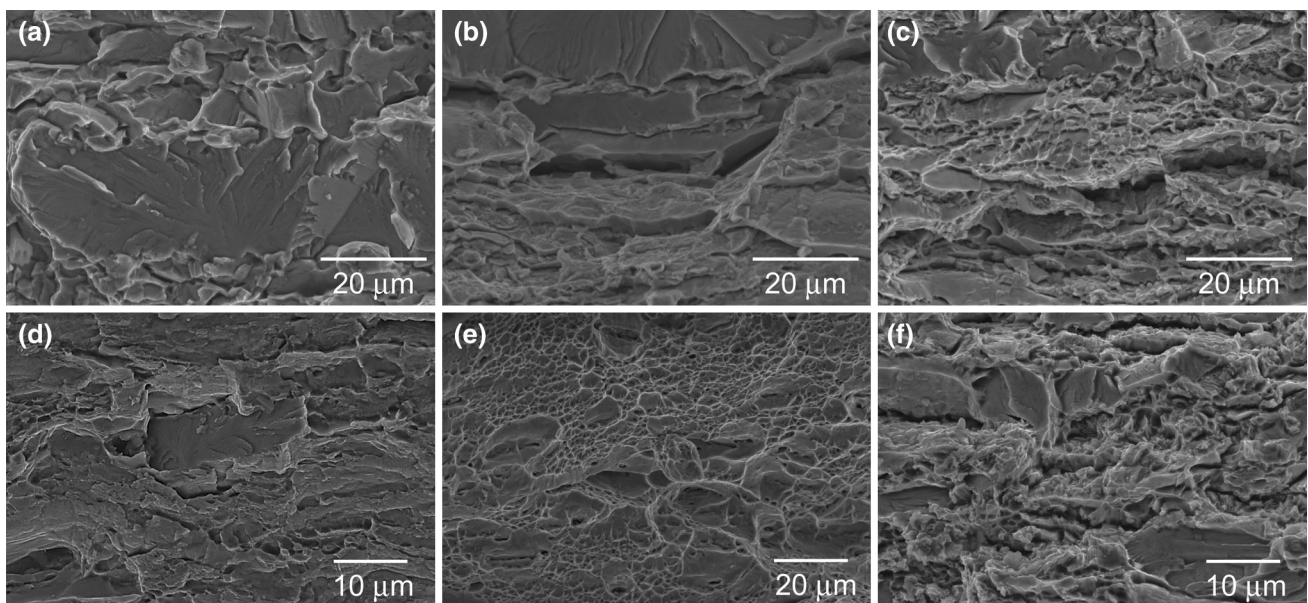


Fig. 6. Fracture surface of alloy A isothermally heat treated for (a) 1 min, (b) 1 h, and (c) 24 h and alloy B for (d) 1 min and (f) 24 h. (e) is locally observed ductile dimples in alloy B heat treated for 1 min.

specimen exhibits considerable ductility, ductile dimples are observed locally as shown in Fig. 6e even though large cleavage facets are also found as shown in Fig. 6c, d, and f, which correspond to alloy A heat treated for 24 h and alloy B for 1 min and 24 h, respectively. Considering the microstructure consisting of coarse ferrite matrix and second phase, the larger cleavage facets with local ductile dimples suggest that the overall elongation of the alloys is strongly dependent on the ductility of second phase because the larger cleavage facets implies that the coarse ferrite is still vulnerable to the propagation of cleavage crack, irrespective of heat treatment condition or alloy chemistry. In other words, the coarse ferrite region manages to be deformed as long as the second phase accommodates the plastic deformation, not generating cracks before necking.

### Influence of Second Phase on Mechanical Properties

The second phase found after isothermal treatment of 1 min is austenite in both alloys A and B, with volume percentages of 9.1% and 19.3%, respectively. The microstructures are similar except for the austenite quantity; however, there is significant difference in elongation, 13.9% and 37.4% for alloy A and B, respectively. It is unlikely that the increase of manganese content has a beneficial effect on the ductility of ferrite matrix in alloy B, but it will affect the characteristics of austenite in terms of the mechanical stability. The austenite in alloys A and B subjected to isothermal treatment of 1 min is metastable because it decomposes gradually into the mixture of ferrite and  $\kappa$ -carbide in prolonged isothermal time. Therefore, the mechanical driving force given by tensile deformation will trigger the deformation-induced martensite transformation in austenite<sup>19</sup> obtained by isothermal treatment of 1 min. In that sense, lower manganese content in alloy A will make the austenite less stable and the formation of brittle martensite at earlier stage of deformation is unavoidable. Figure 7a and b shows the phase map of alloys A and B using EBSD and tensile stage in SEM for direct observation of deformation-induced martensite transformation. It clearly shows that the austenite in alloy A readily transforms into martensite during the course of deformation and the formation of martensite can be recognized at strain of 3.2%, marked by circles. But the austenite in alloy B is so stable that it is insusceptible to the deformation-induced transformation up to strain of 12.1%. As mentioned, the coarse ferrite matrix is vulnerable to the propagation of cleavage fracture, and loss of ductility in second phase by martensite formation will make the alloy sensitive to the brittle fracture. In addition, the deformation-induced martensite transformation is accompanied by volume expansion,<sup>20</sup> which should be accommodated by the surrounding matrix. If the ferrite is not ductile enough as in the

present study, cracks are likely to be generated at the interface.

Dissimilar mechanical behaviors are also found when the microstructure constituent of second phase is a mixture of ferrite and  $\kappa$ -carbide. This corresponds to the alloy A isothermally heat treated for 1 h and 24 h, and alloy B for 24 h. An earlier fracture before necking indicates lack of ductility in alloy A subjected to the heat treatment for 1 h, but the ductility is recovered after isothermal heat treatment for 24 h, exhibiting total elongation around 30%. The alloy B heat treated for 24 h shows comparable elongation as well. From the SEM microstructure in Fig. 3, it is noticed that the ductility is recovered as the morphology of  $\kappa$ -carbide changes from a dense lamellar structure to a round one. To examine the morphological effect on the ductility, the microstructures adjacent to the fracture surface of tensile specimens were observed and shown in Fig. 8. It reveals that the cracks readily traverse the second-phase layer when the morphology of  $\kappa$ -carbide has a fine lamellar structure as indicated by arrows, but many microvoids are formed between carbide and ferrite or by fragmentation of carbide with round morphology. In the latter case, propagation of a sharp crack across the second-phase layer is hardly observed. The occurrence of cracks traversing the dense lamellar structure will have an extremely detrimental effect on the ductility because the cracks are likely to further propagate into the ferrite matrix, which is prone to the cleavage fracture. The reason why this dissimilar deformation and fracture behaviors are involved with the morphology of  $\kappa$ -carbide is not clear yet, but higher stress concentration and inhomogeneous deformation around the lamellar carbide may be one reason. Figure 9 shows the TEM micrographs from a 10% deformed tensile specimen of alloy A. It demonstrates that the distribution of dislocation is localized around the lamellar carbide, but it appears to be more homogeneous with the round shape of carbide, which implies that deformation is conformingly accommodated in the latter case leaving less chance of crack generation.

Finally, it is worth mentioning the propensity of ferrite matrix for cleavage fracture in the investigated alloy. The cleavage fracture occurs when the stress required to move the dislocation is larger than that of cleavage strength.<sup>21</sup> As the lattice friction stress for the movement of dislocation is rapidly increased with decrease of temperature in BCC iron,<sup>22</sup> it showed cleavage fracture at temperature lower than, so-called, ductile-to-brittle transition temperature. Aluminum addition in BCC iron was reported to increase the ductile-to-brittle transition temperature by increasing the yield strength, and caused the cleavage fracture in ferrite even at room temperature with approximate content of 7 wt.%.<sup>23</sup> Therefore, it is natural that the ferrite phase is sensitive to the cleavage fracture when we utilize the massive alloying of aluminum for density

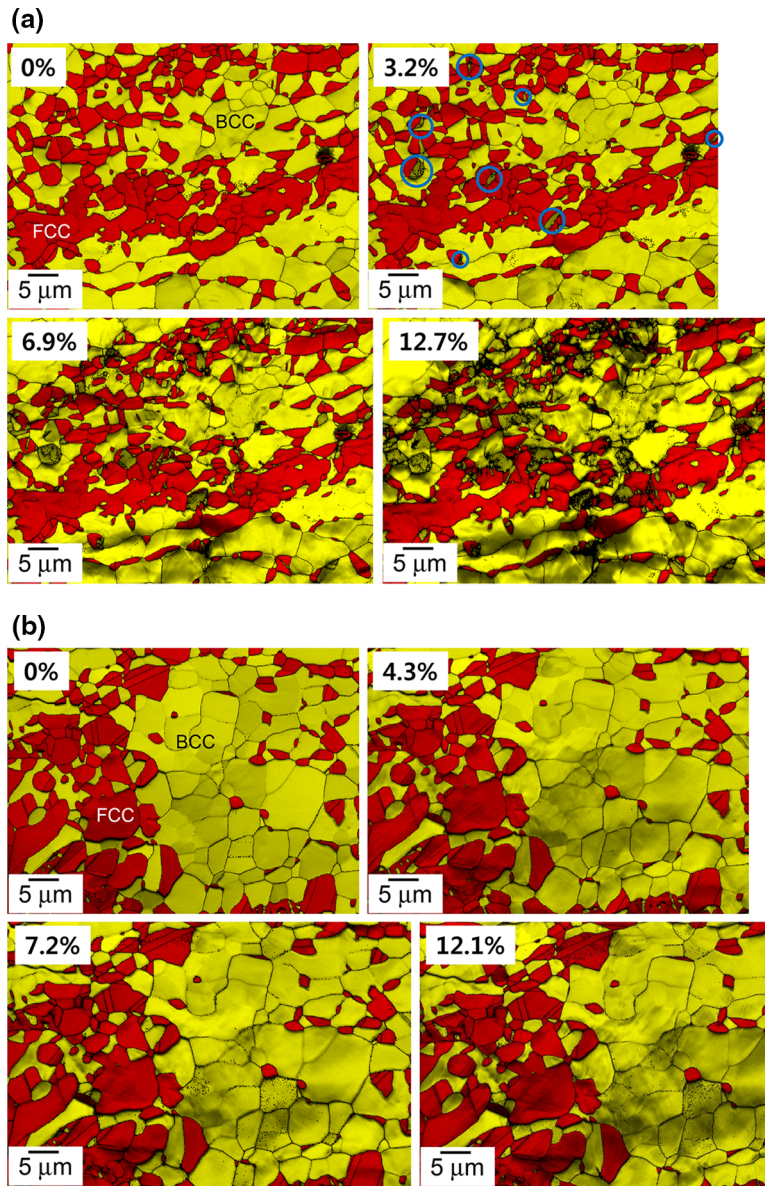


Fig. 7. EBSD phase map showing deformation-induced martensite transformation in (a) alloy A and (b) alloy B subjected to isothermal treatment 1 min. Percentages indicate the tensile strain.

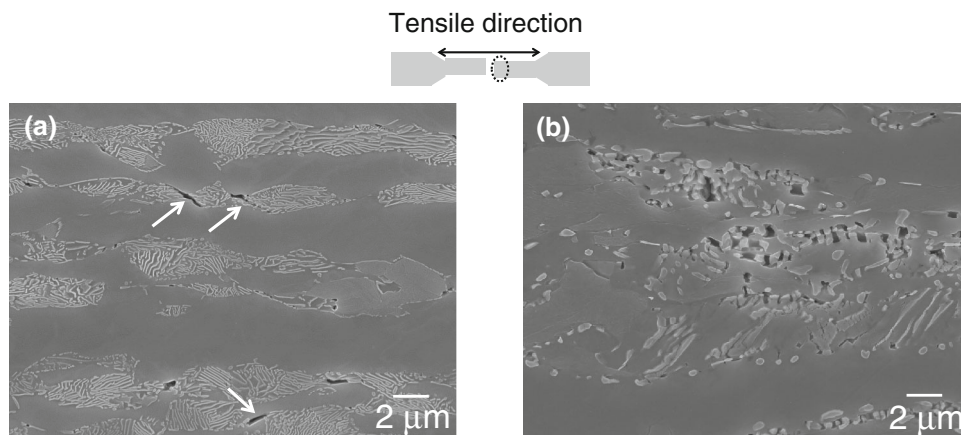


Fig. 8. Microstructure near the fracture surface of tensile specimen of alloy A. Isothermal time is (a) 1 h and (b) 24 h.



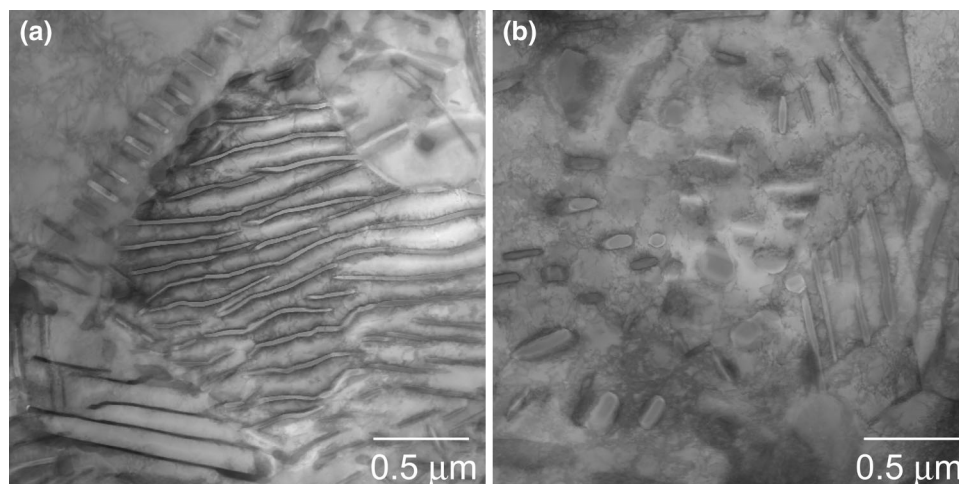


Fig. 9. TEM micrographs from 10% deformed tensile specimens of alloy A. Isothermal time is (a) 1 h and (b) 24 h.

reduction. It suggests that the second phase in aluminum-added low-density steel has such characteristics to avoid the loss of ductility that the occurrence of crack is localized in the second phase and the propagation into the adjacent ferrite matrix phase is effectively suppressed.

### CONCLUSION

The microstructure and mechanical behavior of 0.2C-4Mn-5Al-1Si and 0.2C-8Mn-5Al-1Si multiphase low-density steels have been studied. The following conclusions emerge.

- During the isothermal treatment at 600°C after annealing in two-phase region of ferrite and austenite at 900°C, the austenite is gradually converted into a lamellar structure of ferrite and  $\kappa$ -carbide. The decomposition kinetics of austenite is slower in alloy B containing more manganese.
- The ductility of alloy varies significantly with isothermal treatment condition and alloy chemistry, which indicates that the characteristics of second phase has a critical influence.
- Serious loss of elongation is observed when the characteristics of second phase renders the crack propagate readily in the adjacent ferrite matrix. Regarding this point, mechanically unstable austenite that transformed into martensite at an earlier stage of deformation, and dense lamellar structure of ferrite and  $\kappa$ -carbide, have a detrimental influence on ductility.
- The influence of characteristics of second phase on the ductility of the investigated alloys is associated with the propensity of matrix ferrite for cleavage fracture, which is led by alloying of aluminum.

### ACKNOWLEDGEMENT

This work was supported by the Materials and Components Technology Development Program

(10048157) funded by the Ministry of Trade, Industry and Energy (MOTIE, Korea). Mr. Lee and Prof. Han were supported by the Basic Science Research Program through the National Research Foundation in Korea funded by the Ministry of Science, ICT, and Future Planning (NRF-2013R1A2A2A01008806).

### REFERENCES

1. B.C. De Cooman, *Curr. Opin. Solid State Mater. Sci.* 8, 285 (2004).
2. H. Qu, G.M. Michal, and A.H. Heuer, *Metall. Mater. Trans. A* 44, 4450 (2013).
3. Z. Yu, R. Barabash, O. Barabash, W. Liu, and Z. Feng, *JOM* 65, 21 (2013).
4. D.W. Suh and N.J. Kim, *Scripta Mater.* 68, 337 (2013).
5. H. Kim, D.W. Suh, and N.J. Kim, *Sci. Technol. Adv. Mater.* 14, 014205 (2013).
6. R.A. Howell and D.C. Van Aken, *Iron Steel Technol.* 6, 193 (2009).
7. R. Rana, C. Liu, and R.K. Ray, *Scripta Mater.* 68, 354 (2013).
8. C. Castan, F. Montheillet, and A. Perlade, *Scripta Mater.* 68, 360 (2013).
9. U. Brück, G. Frommeyer, and J. Jimenez, *Steel Res. Int.* 73, 543 (2002).
10. U. Brück and G. Frommeyer, *Steel Res. Int.* 77, 627 (2006).
11. S.J. Park, B. Hwang, K.H. Lee, T.H. Lee, D.W. Suh, and H.N. Han, *Scripta Mater.* 68, 365 (2013).
12. S.S. Sohn, B.J. Lee, S. Lee, N.J. Kim, and J.H. Kwak, *Acta Mater.* 61, 5050 (2013).
13. S.K. Shin, S.J. Park, and K.M. Cho, *J. Korean Soc. Heat Treat.* 26, 306 (2013).
14. G. Frommeyer, E.J. Drewes, and B. Engl, *Revue de Metallurgie-CIT* 97, 1245 (2000).
15. B.C. Cullity, *Elements of X-ray Diffraction*, 2nd ed. (Reading, PA: Addison-Wesley, 1978), pp. 411–415.
16. D.W. Suh, S.J. Park, T.H. Lee, C.S. Oh, and S.J. Kim, *Metall. Mater. Trans. A* 41, 397 (2010).
17. H.K.D.H. Bhadeshia and R.W.K. Honeycombe, *Steels*, 3rd ed. (Oxford, UK: Butterworth-Heinemann, 2006), pp. 71–92.
18. A.W. Wilson, J.D. Madison, and G. Spanos, *Scripta Mater.* 45, 1335 (2001).
19. G.B. Olson and M. Cohen, *Metall. Trans. A* 7, 1905 (1976).

20. S.H. Lee, J.Y. Kang, H.N. Han, K.H. Oh, H.C. Lee, D.W. Suh, and S.J. Kim, *ISIJ Int.* 45, 1217 (2005).
21. G.E. Dieter, *Mechanical Metallurgy*, 3rd ed. (New York, NY: McGraw-Hill International Editions, 1986), pp. 268–269.
22. D. Hull and D.J. Bacon, *Introduction to Dislocations*, 4th ed. (Oxford, UK: Butterworth-Heinemann, 2001), pp. 197–202.
23. J. Herrmann, G. Inden, and G. Sauthoff, *Acta Mater.* 51, 3233 (2003).